NASA Technical Paper 1819

Marking Parts To Aid Robot Vision

John W. Bales and L. Keith Barker

APRIL 1981

NASA

NASA Technical Paper 1819

Marking Parts To Aid Robot Vision

John W. Bales
Tuskegee Institute
Tuskegee, Alabama

L. Keith Barker
Langley Research Center
Hampton, Virginia

NASA
National Aeronautics
and Space Administration

Scientific and Technical
Information Branch

1981

SUMMARY

The premarking of parts for subsequent identification by a robot vision system appears to be beneficial as an aid in the automation of certain tasks, such as construction in space. Accordingly, a simple, color-coded marking system is presented which allows a computer vision system to locate an object, calculate its orientation, and determine its identity. Furthermore, such a system has the potential to operate accurately, and, because the computer shape analysis problem has been greatly simplified, it has the potential to operate in real time.

INTRODUCTION

The use of robots in industry has increased dramatically in the last several years, particularly in Japan but also in this country. A robot is usually a programmable, general purpose arm dedicated to specific tasks. For the most part, these arms are blind. That is, the software controlling most arms makes no use of visual inputs. How to incorporate visual inputs into such software is a problem of much current interest.

One of the most basic tasks of a robot vision system is to locate and identify parts for handling. Four primary problems which must be overcome in order to carry out such a task are noted in the succeeding paragraphs.

The first problem is to distinguish the part from its background. Many sophisticated approaches exist for distinguishing the image of a sought object from its background. However, most approaches require too much computation to allow real-time operation and, in addition, require specially controlled lighting. Any system can be said to operate in real time if it permits the robot arm to operate at an adequate rate. An adequate rate for one situation or operation may be hopelessly slow for others. Since robot arms will, for the immediate future, be operating alongside human workers, any rate which slows down the workers would be inadequate.

The second problem is to determine the orientation of the part. In a precisely controlled situation, the sought part may be prepositioned in the correct orientation. This approach limits the versatility of the system. An adequate vision system should end the necessity of precise placement of parts for the robot arm. However, software for determining the orientation of complex parts can involve excessive computation, slowing real-time operation.

The third problem is to determine the position of the part. In many manufacturing situations this problem is simplified by the fact that the part is on a conveyer belt, the position of which is known. In this situation, a single camera is adequate to provide the information needed to ascertain the position of the part. If the part is not on a conveyer belt and is, in fact, randomly positioned and oriented, some other technique is required. It is

natural to consider the use of two cameras to provide the position information to a robot vision system in this more complex domain. However, the extensive computation required for the cross correlation of two images severely handicaps any two-camera system because of the real-time requirement. Currently, range-finding systems involving a single camera are more promising. Of particular interest is a system first described by Shirai (ref. 1) which uses a single camera and a plane of light as a range finder. In this system a sheet or plane of light is projected toward an object to be identified. The intersection of this plane of light with the object results in a visible light stripe being drawn across the object's surface. This stripe is essentially moved across the surface by panning the plane-of-light generator. The resulting series of light stripes are recorded by a TV camera. Computer software is used to classify sets of straight line segments in these stripes into planes. The object is then recognized by the relationship between these planes. Other plane-of-light systems appear in references 2 and 3. Investigators at the National Bureau of Standards (G. J. VanderBurg, J. S. Albus, and E. Barkmeyer) performed experiments in 1979 in which a plane-of-light vision system was used to successfully acquire an object randomly placed on a table. At present, this type of range-finder system is too slow for real-time operation in three-dimensional space.

The fourth problem is to track the part if it is in motion. Unfortunately, the time required to distinguish the part from its background, determine the orientation of the part, and calculate its position restricts the rate at which the system can track a moving object.

The purpose of this paper is to report on investigations into a vision system capable of handling the previously mentioned problems while requiring only one camera and a minimum of software. For faster execution time, a simple, color-coded marking system eliminates the time-consuming shape analysis required by plane-of-light systems to operate in a three-dimensional environment.

SYMBOLS

A	point on observed object
a	constant
B	point on observed object
C	exact center of circular image
D	centroid of illuminated pixels
d	diameter of cylinder, cm
f	distance from lens center to front image plane, cm
I	diameter of disc image, cm
k	constant

M width of image plane, pixels

m mean value

n image diameter, pixels

P lens center

$\tilde{P}$ hypothetical reflection of point P

P_1, P_2, P_3, P_4, P_5 point locations on cylinder

R^* range from lens center to object projection on principal ray, cm

$r, r_1, r_2, r_3, r_4, r_5$ range from lens center to point on object, cm

$r(A), r(B)$ range from lens center to points A and B, respectively, cm

S diameter of disc, cm

S_1, S_2, S_3, S_4, S_5 dot locations on observed object

$\vec{u}$ unit vector

$\vec{u}_A, \vec{u}_B$ unit vectors from P toward A and B, respectively

W width of image plane, cm

w, w_1, w_2 spacing between marks on observed object, cm

x, y rectangular coordinates in image plane

x_c, y_c exact center of circular image

x_i, y_i coordinates of center of ith illuminated pixel

$\bar{x}, \bar{y}$ centroid coordinates of illuminated pixels

α_1, α_2 angles used to compute rotation angle ψ for cylinder, deg

γ angular field of view measured on diagonal of image plane, deg

δ tilt angle away from perpendicular to line of sight, deg

θ angular separation between rays emanating from P through A' and B', deg

$\theta_1, \theta_2, \theta_3, \theta_4$ angular separation of surface markings, deg

σ least squares fit of σ_n, pixels or cm

σ_n standard deviation of $\bar{x} - x_c$ computed from random data of circular disc diameter n, pixels

σ_r standard deviation of error in r, cm

σ_δ standard deviation of error in δ, deg

ϕ angle between two range vectors to points on observed object, deg

ψ rotation angle of cylinder about its longitudinal axis, deg

Mathematical notation:

$||$ length or magnitude

$\cdot$ dot product

$\overrightarrow{AB}$ vector from A to B

$\approx$ approximation

A prime (') over a symbol denotes a projection of that point in the image plane.

ANALYSIS

Marking System

All vision systems to date, at least the ones of which the authors are aware, identify parts by analyzing their shapes. If the shape is complex and if the part is presented to the camera randomly positioned and oriented, the process of analysis is complicated and computation time is increased. One solution to this problem is to place an identifying mark or symbol on each part at a sufficient number of locations for visibility from any side. Furthermore, because the geometry of the mark is known and is less complex than the geometry of the part, less software is required to deduce the range and orientation of the part. The most parsimonious mark would be one from which could be deduced range, orientation, and a third parameter to identify which part the mark is on. Additional parameters would require more complex marks. However, there is still the problem of distinguishing the mark from the background. This problem could be simplified by using marks of specific complementary colors (two colors whose combination produce white) which could be enhanced with color filters. For example, denote the complementary colors as color 1 and color 2. If the mark is a color 1 disk and color 1 and color 2 filters are placed alternately in front of the camera lens, the color 1 spot will appear as a flashing disc while the rest of the image remains relatively unchanged. By subtracting alternate images, the disc is greatly enhanced relative to the rest of the image.

To illustrate this concept, an investigation has been made into possible marks for two general classes of objects: cylindrical objects and objects with

a flat surface. The marks investigated which give range (R) and orientation (O), plus a given number of extra parameters (N), will be referred to as RO + N marks.

RO + 1 Mark for Cylinders

The RO + 1 mark for a cylinder could consist of two stripes placed radially around the cylinder with both stripes connected by a third which spirals once around the cylinder (fig. 1). The spiral stripe and one radial stripe are the same color, while the other radial stripe is the complement of that color to resolve any ambiguity in the direction. This marking scheme is used in an approximate way to find the range and orientation of the cylinder, plus the diameter of the cylinder. The diameter is encoded by spacing the two circular stripes so that the width of the space times the diameter of the cylinder is a predetermined constant.

Image plane.- In figure 2, the image plane is depicted as a matrix of light sensitive elements called pixels. Actually, the image plane shown in figure 2 is an imaginary front image plane introduced for convenience by workers in computer graphics and machine perception to display the image in an upright position. The real image plane is located behind the lens center and gives an inverted image. Image coordinates in the two planes are related simply by a multiplicative factor of minus unity. The lens center is located at a known distance from the image plane on the principal ray, which is perpendicular to the image plane.

Angular separation of image points.- If the coordinates of two points A' and B' in the image plane (shown in fig. 3) are known and the coordinates of P are known, the angular separation θ between the rays emanating from P through A' and B' can be found from the definition of the dot product as

$$\cos \theta = \frac{\overrightarrow{PA'} \cdot \overrightarrow{PB'}}{\left|\overrightarrow{PA'}\right| \left|\overrightarrow{PB'}\right|} \tag{1}$$

In a camera, P is the lens center which is known in advance, and A' and B' are directly measurable in the image plane coordinate system (fig. 2).

Diameter and range.- Shown in figure 4(a) is the portion of a cylinder with the two circular stripes and the separation distance w between these stripes. The image plane in front of the lens center P is not shown. The points P_1 and P_2 are points where P would be located if it were shifted parallel to the cylinder's axis to a point lying in the plane of the circular stripes. Assuming that P is located at P_1 leads to the geometry of figure 4(b). However, the circular stripe and P are not really coplanar; therefore, use of figure 4(b) instead of figure 4(a) results in the approximation

$$r_1 \approx \frac{d}{2} \csc\left(\frac{\theta_1}{2}\right) \tag{2}$$

where d is the momentarily unknown diameter of the cylinder. The angle θ_1 can be found using equation (1), where the points A' and B' are the end points of the visible circular arc on the image plane. In a similar manner, the approximate equation for r_2 is

$$r_2 \approx \frac{d}{2} \csc\left(\frac{\theta_2}{2}\right) \tag{3}$$

Referring to figure 4(c), notice that by the law of cosines

$$w^2 = r_1^2 + r_2^2 - 2r_1 r_2 \cos\phi \tag{4}$$

By assumption, the product of the width w and diameter d is a predetermined constant k, so that

$$w = \frac{k}{d} \tag{5}$$

Substituting equations (2), (3), and (5) into equation (4) gives

$$\frac{k^2}{d^2} \approx \frac{d^2}{4} \csc^2\left(\frac{\theta_1}{2}\right) + \frac{d^2}{4} \csc^2\left(\frac{\theta_2}{2}\right) - \frac{d^2}{2} \csc\left(\frac{\theta_1}{2}\right) \csc\left(\frac{\theta_2}{2}\right) \cos\phi \tag{6}$$

in which only d is unknown. Solving for d yields

$$d \approx \left[\frac{4k^2}{\csc^2\left(\frac{\theta_1}{2}\right) + \csc^2\left(\frac{\theta_2}{2}\right) - 2 \csc\left(\frac{\theta_1}{2}\right) \csc\left(\frac{\theta_2}{2}\right) \cos\phi}\right]^{1/4} \tag{7}$$

This value of d may then be substituted into equations (2) and (3) to solve for r_1 and r_2. Hence, both range and cylinder diameter are found.

Direction cosines of cylinder's axis.- In figure 5, A and B are points in the field of view whose ranges are known. Let $r(A) = |\overrightarrow{PA}|$ and $r(B) = |\overrightarrow{PB}|$. Then, the orientation of $\overrightarrow{AB}$ is specified by the unit vector

$\vec{u} = \dfrac{\vec{AB}}{\left|\vec{AB}\right|}$ whose coordinates are the direction cosines of $\vec{AB}$. Let

$$\vec{u}_A = \frac{\vec{PA}'}{\left|\vec{PA}'\right|} \tag{8}$$

and

$$\vec{u}_B = \frac{\vec{PB}'}{\left|\vec{PB}'\right|} \tag{9}$$

then

$$\vec{AB} = r(B)\vec{u}_B - r(A)\vec{u}_A \tag{10}$$

so

$$\vec{u} = \frac{r(B)\vec{u}_B - r(A)\vec{u}_A}{\left|r(B)\vec{u}_B - r(A)\vec{u}_A\right|} \tag{11}$$

This procedure is applied to figure 6 to obtain the direction cosines of the cylinder's axis.

Rotation of cylinder about its axis.- The orientation of the cylinder can be specified by the direction cosines of the cylinder axis and by an angle between 0^o and 360^o, to indicate the amount of rotation about that axis. Figure 7 is used to examine rotation. The imaginary line 2 in figure 7 is parallel to the cylinder axis and indicates that points P_1 and P_3 are lined up with some distinctive feature of the cylinder, such as the notch shown. Traveling from P_1 to P_3 via the spiral stripe represents a rotation of 360^o, so traveling from P_1 to P_2 represents some fraction of 360^o, which is equivalent to the amount of rotation. The angle ψ indicates the amount of rotation about the axis with respect to an imaginary line 1, which is parallel to the cylinder axis. For example, if the points P_2, P_5, and P_1 are coincident, then $\psi = 0^o$; and if P_2, P_4, and P_3 are coincident, then $\psi = 360^o$. The angle ψ is given exactly by

$$\psi = \frac{\left|\overrightarrow{P_2P_5}\right|}{\left|\overrightarrow{P_4P_5}\right|}(360^o) \tag{12}$$

where $\left|\overrightarrow{P_2P_5}\right|$ and $\left|\overrightarrow{P_4P_5}\right|$ are line segment lengths. In this development, equation (12) is approximated by

$$\psi \approx \left(\frac{\alpha_1}{\alpha_1 + \alpha_2}\right)360^o \tag{13}$$

The angles α_1 and α_2 can be approximated as follows. The arc portion of the circular stripe 1 will appear on the image plane, which is not shown in figure 7. The point P_5' is approximated by the point in the image plane which corresponds to a point halfway between the two end points of the arc. Point P_4' is similarly approximated. Line 1 is then approximated by the straight line connecting these two approximations of the image points P_4' and P_5'. Now, the spiral stripe will cause a set of pixels to be illuminated in the image plane. Common pixel points of line 1 and the spiral stripe locate P_2'. Since the image points P_4', P_2', and P_5' are known, the angular separations α_1 and α_2 are computed as θ was in equation (1).

RO + N Mark for Flat Surfaces

Shown in figure 8(a) is a widget with three circular spots equally spaced in a straight line. One of the end spots is the complementary color of the other two, to establish direction. In figure 8(b), S_1, S_2, and S_3 denote the three spots on the part. The angles θ_1 and θ_2 are found using equation (1). The triangle PS_1S_3 is extended to a parallelogram $PS_1\tilde{P}S_3$ to illustrate the equations which follow.

Let $r_1 = \left|\overrightarrow{PS_1}\right|$, $r_2 = \left|\overrightarrow{PS_2}\right|$, and $r_3 = \left|\overrightarrow{PS_3}\right|$. Then, if w_1 is the width between spots, the law of cosines applied to the triangle PS_1S_2 gives

$$w_1^2 = r_1^2 + r_2^2 - 2r_1r_2 \cos\theta_1 \tag{14}$$

and, using PS_2S_3,

$$w_1^2 = r_2^2 + r_3^2 - 2r_2r_3 \cos\theta_2 \tag{15}$$

By applying the identity $\sin(180^o - \theta) = \sin\theta$ and the law of sines on the triangle $PS_1\tilde{P}$ it follows that

$$\frac{r_1}{\sin \theta_2} = \frac{r_3}{\sin \theta_1} = \frac{2r_2}{\sin (\theta_1 + \theta_2)} \tag{16}$$

In equations (14), (15), and (16), the quantities θ_1, θ_2, and w_1 are known, and r_1, r_2, and r_3 are unknown. From equation (16),

$$r_1 = \frac{2r_2 \sin \theta_2}{\sin (\theta_1 + \theta_2)} \tag{17}$$

and

$$r_3 = \frac{2r_2 \sin \theta_1}{\sin (\theta_1 + \theta_2)} \tag{18}$$

Substituting equation (17) into equation (14), or substituting equation (18) into equation (15), leaves r_2 as a function of w_1, θ_1, and θ_2. The resulting equation in either situation can be expressed as

$$r_2 = \frac{w_1 \sin (\theta_1 + \theta_2)}{\sqrt{\sin^2 (\theta_1 - \theta_2) + 4 \sin^2 \theta_1 \sin^2 \theta_2}} \tag{19}$$

Then, r_1 and r_3 are found by substituting equation (19) into equations (17) and (18). The direction cosines can now be found by the same procedure used in equations (8) to (11), remembering that the images S_1', S_2', and S_3' are directly measurable on the image plane.

There is insufficient information to deduce the rotation of the part in figure 8(b) about the S_1S_3 axis. A set of three spots perpendicular to the original three could resolve this ambiguity and, coincidentally, allow the encoding of an additional parameter. One way to construct such a RO + 1 mark is shown in figure 9(a) with the orthogonal sets of spots sharing a center spot. In figure 9(b), the product of the distances w_1 and w_2 from the center spot to alternate corner spots is a prespecified constant k, that is, $w_1w_2 = k$. Spots S_1, S_2, and S_3 in figure 9 lead to equations (17), (18), and (19). Similarly, spots S_4, S_2, and S_5 in figure 9 lead to the following equations:

$$r_4 = \frac{2r_2 \sin \theta_4}{\sin (\theta_3 + \theta_4)} \tag{20}$$

$$r_5 = \frac{2r_2 \sin \theta_3}{\sin (\theta_3 + \theta_4)} \tag{21}$$

$$r_2 = \frac{w_2 \sin (\theta_3 + \theta_4)}{\sqrt{\sin^2 (\theta_3 - \theta_4) + 4 \sin^2 \theta_3 \sin^2 \theta_4}} \tag{22}$$

where r_4, r_5, θ_3, and θ_4 are shown in figure 9(c).

Multiplying equations (19) and (22) gives an equation for r_2^2 in terms of the known product $w_1 w_2 = k$ and trigonometric functions of the angles θ_1, θ_2, θ_3, and θ_4. Taking the square root gives r_2. Then, w_1 and w_2 can be found by using equations (19) and (22), respectively. The ratio $\frac{w_1}{w_2}$ represents an additional parameter which can be used to identify a particular part. Furthermore, the direction cosines can now be found for two orthogonal vectors $\overrightarrow{S_2S_4}$ and $\overrightarrow{S_2S_3}$, lying on the flat surface containing the mark. This is enough information to completely specify the orientation of the part.

The configuration of a RO + 2 mark for flat surfaces is shown in figure 10. The corner spot automatically provides the direction of the mark freeing the complementary colors for use as a binary code for each of the five spots. This provides an additional parameter with 32 discrete values (each of the five spots can be either of two colors), in addition to the $\frac{w_1}{w_2}$ parameter. An equivalent "T" shaped mark could also be used.

ERROR ANALYSIS

From a geometrical standpoint the RO marks discussed here are fully adequate for the purpose of finding the direction, range, and orientation of a given part. However, inaccuracies of measurement must be taken into account in an actual system. The determination of range in equations (2), (3), and (17) to (22) involves the accurate determination of separation angles from equation (1). But, separation angles cannot be determined exactly, because it is not possible to find the exact center of an image in the image plane. In order to investigate this problem it was assumed that the image plane consisted of a rectangular array of picture elements, or pixels. In figure 11, the image of a circular disc is seen on the image plane. If a given pixel is illuminated sufficiently to exceed some predetermined threshold value, it is said to be "illuminated." In order to simplify this aspect of the problem it is assumed that a given pixel is illuminated if its center falls within the boundary of the image; otherwise, it is assumed not to be illuminated. In figure 11, the shaded squares represent the illuminated pixels. The center of the image is C and the center of the collection of illuminated pixels is D. Let the sequence (x_1,y_1), (x_2,y_2), . . ., (x_k,y_k) denote the centers of the illuminated pixels.

If

$$\bar{x} = \frac{1}{k} \sum_{i=1}^{k} x_i \tag{23}$$

and

$$\bar{y} = \frac{1}{k} \sum_{i=1}^{k} y_i \tag{24}$$

then $D = (\bar{x},\bar{y})$ is the centroid of the illuminated pixels. If $C = (x_c,y_c)$, then

$$D - C = (\bar{x} - x_c, \bar{y} - y_c) \tag{25}$$

is the deviation of the centroid from the true center of the image.

For a circular image with a diameter given in n pixels and a given location of its center C on some pixel, $D - C$ can be exactly determined analytically. In fact, though, the center C is known only in a statistical sense, because it is randomly placed somewhere within a given pixel. Thus, $D - C$ would be a random variable. For the purpose of this study, the random variable $\bar{x} - x_c$ from equation (25) was investigated first and the results subsequently applied to $\bar{y} - y_c$ and $D - C$. The circular discs used as images were assumed to have diameters which varied from 2 to 50 pixels. For each specific image diameter, 100 choices of C were selected uniformly at random within a given pixel. For each choice of n, 100 samples of $\bar{x} - x_c$ were computed. The mean m and the standard deviation σ_n of these 100 samples are shown in table I. The units of these statistics could be measured in actual distances, such as centimeters; however, the statistical values would vary, depending upon the particular dimensions of the imaging device. Therefore, m and σ are measured in pixel units. The n in table I denotes image diameter in pixels. Because the values of m were consistently small and no trend was apparent, it was assumed that $m = 0$. The assumption is made that σ is inversely proportional to the square root of n; that is,

$$\sigma = \frac{a}{\sqrt{n}} \tag{26}$$

The best value of a, in the least-squares sense, is

$$a = \frac{\sum_{n=2}^{50} \frac{\sigma_n}{n}}{\sum_{n=2}^{50} \frac{1}{n}} \tag{27}$$

Application of equation (27) to the values of σ_n in table I yields

$$\sigma = \frac{0.222}{\sqrt{n}} \tag{28}$$

For later reference, the equation for 2σ is

$$2\sigma = \frac{0.444}{\sqrt{n}} \tag{29}$$

In figure 12, the values of σ_n in table I and the approximation σ in equation (28) are plotted in percent as functions of circular image diameter n. Because the fit is apparently a good one, equation (28) is taken as a good estimate of the standard deviation of $\bar{x} - x_c$ as a function of image diameter n. In agreement with reference 4, the accuracy of predicting the center of the circular image improves as the image size increases.

The length of the error vector in equation (25) is

$$|D - C| = \sqrt{(\bar{x} - x_c)^2 + (\bar{y} - y_c)^2} \tag{30}$$

Substituting $\bar{x} - x_c = 2\sigma$ and $\bar{y} - y_c = 2\sigma$ into equation (30) and using equation (29) gives

$$|D - C| = \frac{0.628}{\sqrt{n}} \tag{31}$$

as an approximation to the maximum length of the error vector.

The location error of the circular image center for equations (29) and (31) is shown in figure 13 along with numerical solutions for the approximate maximum error for discrete points computed in reference 4. Equation (29) represents a 2σ error in either the x- or y-direction. Equation (31) represents an approximation to the maximum error for 2σ variations in both the x- and y-directions. In general, equation (31) gives a conservative estimate of the maximum error for the diameters considered in figure 13. As expected, the estimate given by equation (29) is low due to limiting to only one direction.

The n in equation (28) can be related to physical parameters in figures 14 and 15. Figure 14 shows the disc with diameter S in centimeters and its image with diameter I in centimeters. By similar triangles,

$$\frac{I}{2f} = \frac{S}{2R^*} \tag{32}$$

or

$$I = \frac{fS}{R^*} \tag{33}$$

The ratio of the disc image diameter n in pixels to the width of the image plane M in pixels is equal to the ratio of the disc image diameter I in centimeters to the width of the image plane W in centimeters. Hence,

$$\frac{n}{M} = \frac{I}{W} \tag{34}$$

or

$$n = I \frac{M}{W} \tag{35}$$

Substituting equation (33) into equation (35) gives

$$n = \frac{fS}{R^*} \frac{M}{W} \tag{36}$$

The f in equation (36) can be expressed as a function of the field-of-view angle γ and width W of the image plane in figure 15 as

$$\cot\left(\frac{\gamma}{2}\right) = \frac{f}{W}\sqrt{2} \tag{37}$$

or

$$f = \frac{W}{\sqrt{2}} \cot\left(\frac{\gamma}{2}\right) \tag{38}$$

where γ is the field of view measured on the diagonal of the image plane. Substitute equation (38) into equation (36) to obtain

$$n = \frac{SM}{R^*\sqrt{2}} \cot\left(\frac{\gamma}{2}\right) \tag{39}$$

Equation (39) can be used to express equation (28) as

$$\sigma = 0.264\sqrt{\frac{R^* \tan(\gamma/2)}{MS}} \tag{40}$$

To convert σ from pixel units to centimeters, multiply by the scale factor W/M to get

$$\sigma = (0.264)\frac{W}{M}\sqrt{\frac{R^* \tan(\gamma/2)}{MS}} \tag{41}$$

In figure 11, it is assumed that $D - C = (\bar{x} - x_c, \bar{y} - y_c)$ is a random variable satisfying a bivariate normal distribution with each variable having mean $m = 0$ and standard deviation σ satisfying equation (41). For a given charge-coupled-device (CCD) imaging chip, the values of M and W may be different in the x- and y-directions, giving different values of σ in the x- and y-directions.

The accuracy with which the range and orientation may be computed is determined for a sample problem by assuming that, in equation (41), $W = S = 0.625$ and $M = 256$ in both the x- and y-directions. In other words, the imaging surface is square with sides W equal to 0.625 centimeter, the imaging surface is composed of a matrix of 256 by 256 pixels ($M = 256$), and the diameter of the disc mark S is 0.625 centimeter. Thus, equation (41) becomes

$$\sigma = (5.00 \times 10^{-5}) \sqrt{R^* \tan (\gamma/2)} \tag{42}$$

The three-dot marking in figure 8 suffices for testing range accuracy from equations (17), (18), and (19) and tests the aspect of orientation most susceptible to errors; namely, the amount of tilt δ away from a perpendicular to the line of sight (fig. 16). To further simplify the analysis, it was assumed that the image of the mark lies horizontally in the image plane (fig. 17). Errors were calculated in range and tilt for range values from 50 cm to 150 cm in 25-cm increments and for tilt values from 5° to 85° in 20° increments. Wide-angle (45°) and narrow-angle (5°) fields of view were used. For each choice of parameters, 1000 uniformly random choices were made within the entire image plane for the coordinates of the image of the center spot (fig. 17). For each of these 1000 choices, the true positions of the three images were altered in the x- and y-directions by a normal random variable with mean $m = 0$ and σ determined by equation (42). Of course, the three image spots will not always be simultaneously visible in the window assumed for the center spot, especially for the smaller field of view ($\gamma = 5^\circ$); however, this difficulty is separate from the problem of determining the accuracy of the measured tilt when it is measurable.

The range and tilt were then calculated using the altered positions of the images and the differences from the true values were calculated. The mean and standard deviation of these differences were calculated for each combination of range, tilt, and field-of-view parameters. The results are shown in tables II and III.

The results for the narrow (5°) field of view are good, suggesting that the range and orientation of a part can be determined fairly accurately when the tilt is not more than 45° and the range is not more than 125 cm. The results for the wide field of view (45°) are less encouraging and suggest that a wide-angle lens should only be used to locate the mark, after which the camera should switch to a narrow-angle lens.

Inherent in the error analysis are the approximating assumptions that the plane of each disc is parallel to the image plane and that each disc projects as a circle on the image plane. A more thorough error analysis is needed to examine the implications of these simplifying assumptions.

CONCLUDING REMARKS

Having a robot view the three-dimensional world as man views it is only a dream at present; however, much headway has been made in this direction and current research efforts are attacking the problems involved. While generic work in automated computer vision is proceeding, there are foreseeable applications, such as construction in space, which can use intermediate or simplified vision systems.

In general, computer vision systems identify parts by analyzing their shapes. However, the premarking of parts for subsequent identification by a robot vision system appears to be beneficial as an aid in the automation of certain tasks. Accordingly, a simple, color-coded marking system is presented in this paper which allows a computer vision system to locate an object, calculate its orientation, and determine its identity. Such a system has the potential to operate accurately, and, because the computer shape analysis problem has been greatly simplified, it has the potential to operate in real time.

Langley Research Center
National Aeronautics and Space Administration
Hampton, VA 23665
February 9, 1981

REFERENCES

1. Shirai, Yoshiaki: Recognition of Polyhedrons With a Range Finder. Pattern Recognition, vol. 4, 1972, pp. 243-250.

2. Nevatia, Ramakant; and Binford, Thomas O.: Description and Recognition of Curved Objects. Artif. Intell., vol. 8, 1977, pp. 77-98.

3. Popplestone, R. J.; and Ambler, A. P.: Forming Body Models From Range Data. D.A.I. Res. Rep. No. 46, Dep. Artif. Intell., Univ. Edinburgh, Oct. 1977.

4. McVey, E. S.; and Jarvis, G. L.: Ranking of Patterns for Use in Automation. IEEE Trans. Ind. Electron. & Control Instrum., vol. IECI-24, no. 2, May 1977, pp. 211-213.

TABLE I.- VARIATION OF STATISTICS OF $\bar{x} - x_c$ WITH PIXEL DIAMETER OF DISC

n, pixels	m, pixels	σ_n, pixels	n, pixels	m, pixels	σ_n, pixels
1	------	-----	26	-0.003	0.041
2	-0.015	0.168	27	-.003	.050
3	-.005	.133	28	-.002	.035
4	.002	.103	29	.004	.041
5	.009	.109	30	-.001	.039
6	.002	.091	31	.001	.036
7	.008	.082	32	-.004	.039
8	-.002	.085	33	-.004	.032
9	-.002	.064	34	-.003	.044
10	.003	.065	35	-.001	.036
11	-.008	.061	36	.003	.033
12	.005	.062	37	.010	.036
13	-.004	.067	38	.002	.033
14	-.001	.055	39	.000	.041
15	-.001	.061	40	-.002	.033
16	-.010	.052	41	-.001	.032
17	-.002	.059	42	.004	.033
18	-.007	.052	43	-.002	.032
19	-.006	.048	44	.001	.035
20	-.006	.053	45	-.002	.030
21	-.002	.043	46	-.003	.029
22	.000	.048	47	-.001	.031
23	-.001	.048	48	-.004	.030
24	-.011	.042	49	.005	.032
25	-.001	.042	50	.000	.026

TABLE II.- ERROR IN CALCULATED TILT ANGLE AND RANGE FOR 5° FIELD OF VIEW ($\gamma = 5^{\circ}$)

Actual tilt angle, δ, deg	Error in calculated tilt angle		Actual range, r, cm	Error in calculated range	
	m_{δ}, deg	σ_{δ}, deg		m_r, cm	σ_r, cm
5	0.0	0.0	50	0.00	0.00
	.0	.0	75	.00	.00
	.0	.1	100	.00	.00
	.0	.2	125	.00	.00
	.0	.3	150	.00	.00
25	0.0	0.0	50	0.00	0.00
	.0	.0	75	.00	.00
	.0	.1	100	.00	.00
	.0	.2	125	.00	.25
	.0	.3	150	.00	.25
45	0.0	0.0	50	0.00	0.00
	.0	.0	75	.00	.00
	.0	.1	100	.00	.25
	.0	.2	125	.00	.25
	.0	.3	150	.00	.75
65	0.0	0.0	50	0.00	0.00
	.0	.0	75	.00	.25
	.0	.1	100	.00	.25
	.0	.2	125	.00	.75
	.0	.3	150	.00	1.50
85	0.0	0.0	50	0.00	0.25
	.0	.0	75	.00	.75
	.0	.1	100	.00	1.75
	.0	.2	125	.00	4.00
	.0	.3	150	.25	7.75

TABLE III.- ERROR IN CALCULATED TILT ANGLE AND RANGE FOR 45° FIELD OF VIEW (γ = 45°)

Actual tilt angle, δ, deg	Error in calculated tilt angle		Actual range, r, cm	Error in calculated range	
	m_δ, deg	σ_δ, deg		m_r, cm	σ_r, cm
5	0.0	0.4	50	0.00	0.00
	.0	1.2	75	.00	.25
	.0	2.4	100	.00	.50
	.0	4.4	125	-.50	1.00
	.0	6.9	150	-1.00	2.25
25	0.0	0.4	50	0.00	0.25
	-.1	1.2	75	.00	.75
	-.1	2.4	100	.00	2.00
	-.3	4.4	125	.00	4.25
	-1.0	6.7	150	.25	7.75
45	0.0	0.4	50	0.00	0.25
	.0	1.2	75	.00	1.50
	-.1	2.4	100	.00	4.00
	-.4	4.3	125	.50	9.00
	-.5	6.9	150	.25	17.00
65	0.0	0.4	50	0.00	0.75
	.0	1.2	75	.00	3.25
	-.2	2.5	100	.50	9.25
	-.4	4.7	125	1.25	21.25
	-1.7	7.8	150	8.00	39.75
85	-0.1	0.5	50	0.75	4.25
	-.3	1.4	75	4.00	21.00
	-5.2	22.0	100	49.75	168.50
	-20.5	49.3	125	108.00	280.75
	-36.5	66.4	150	95.50	305.75

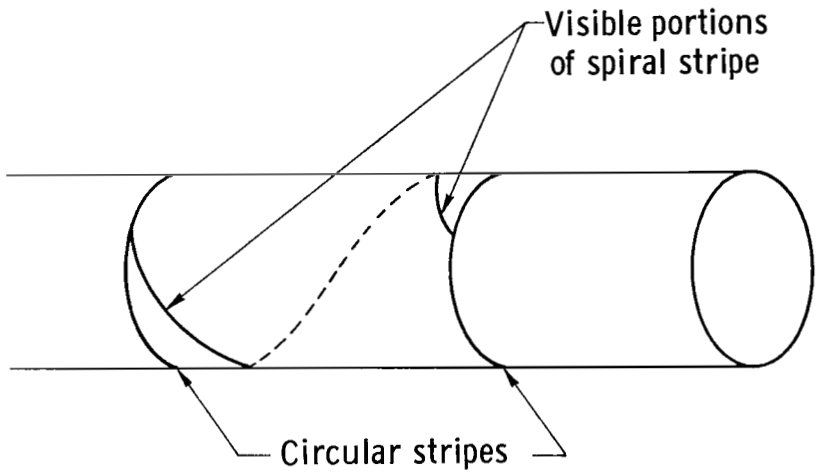

Figure 1.- RO + 1 mark for cylinders.

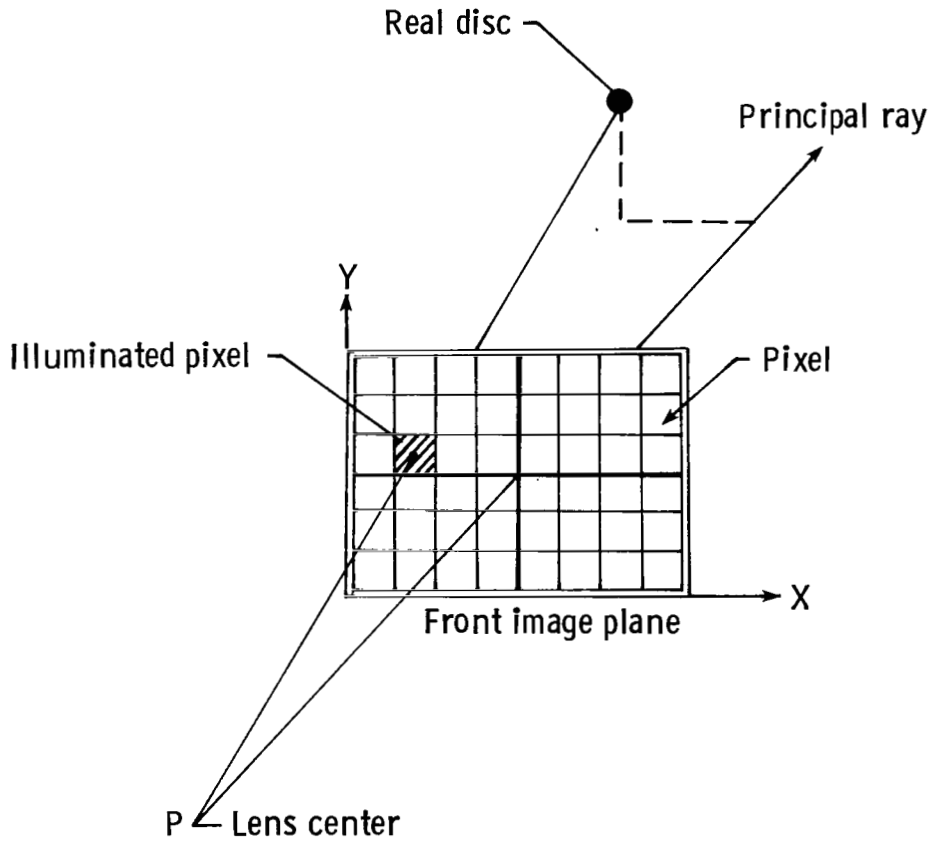

Figure 2.- Array of pixels (light-sensitive elements).

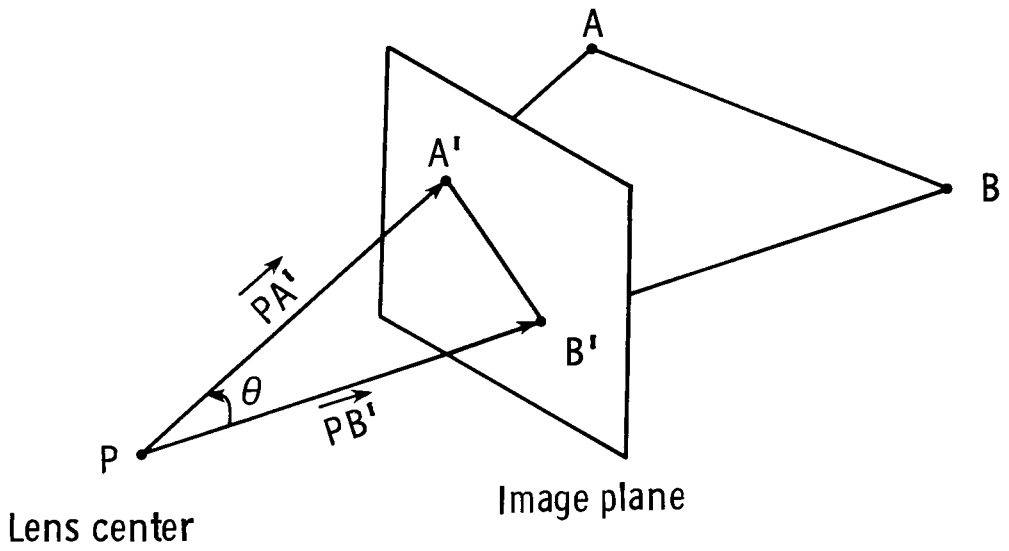

Figure 3.- Angular separation of image points.

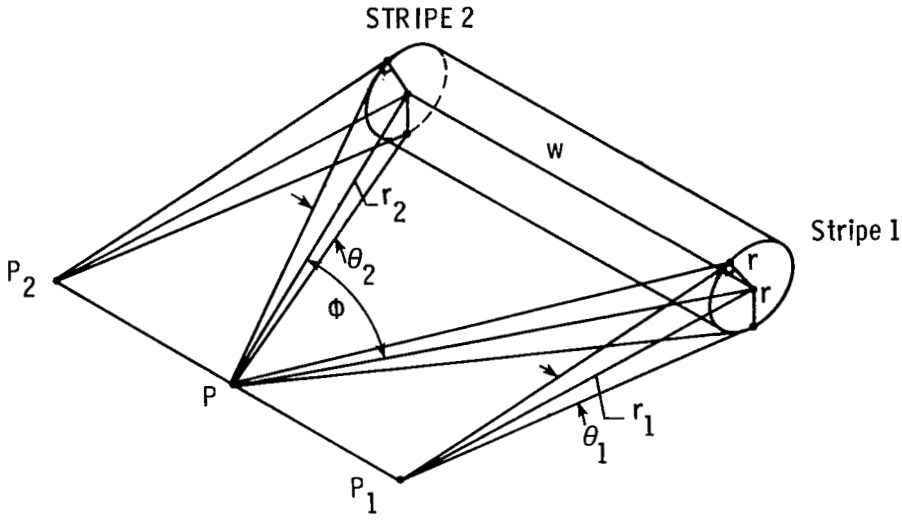

(a) Location of lens center P relative to stripes.

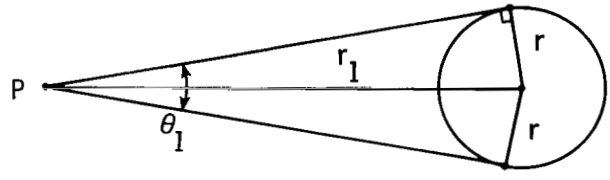

(b) Assuming that P is located at P_1.

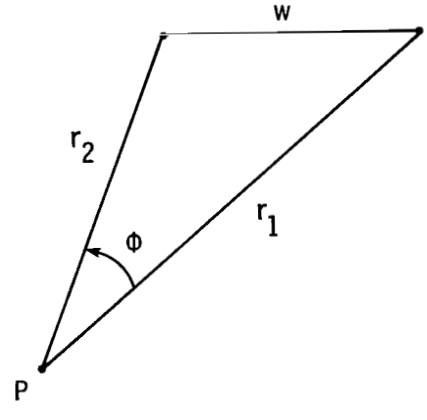

(c) Separation of stripes.

Figure 4.- Coded stripes on cylinder.

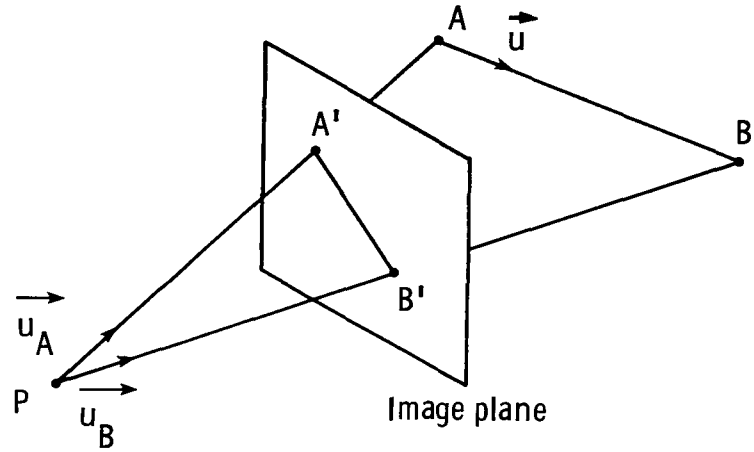

Figure 5.- Orientation of two points with known ranges.

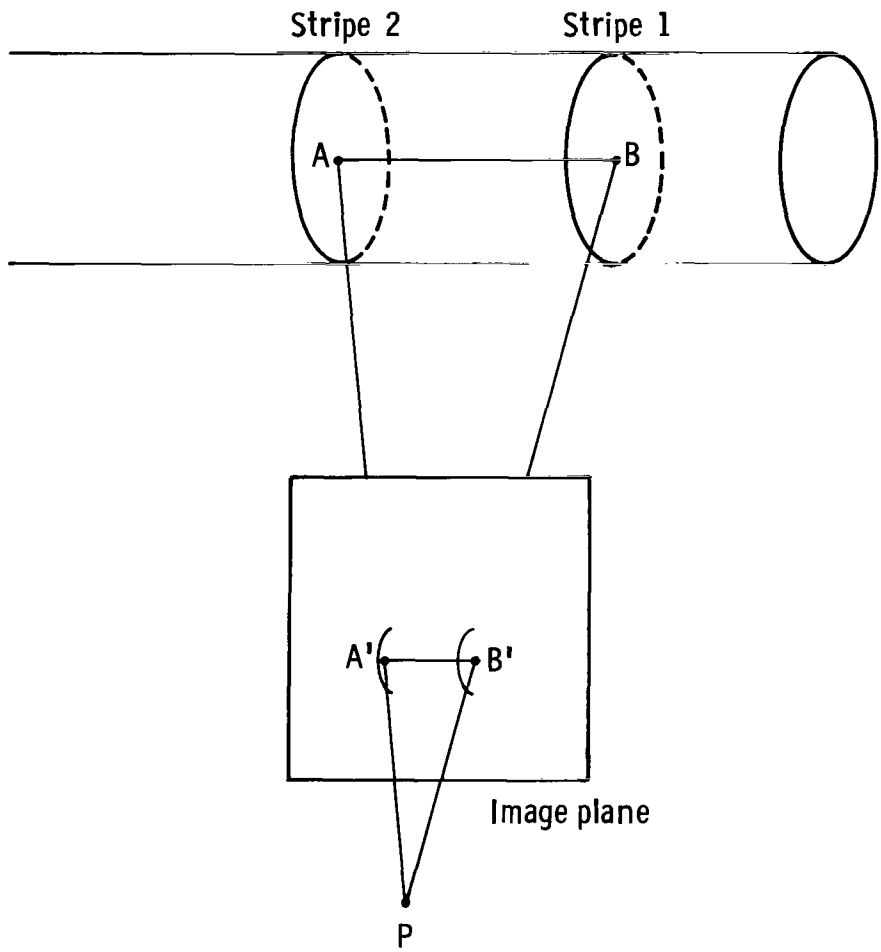

Figure 6.- Orientation of cylinder.

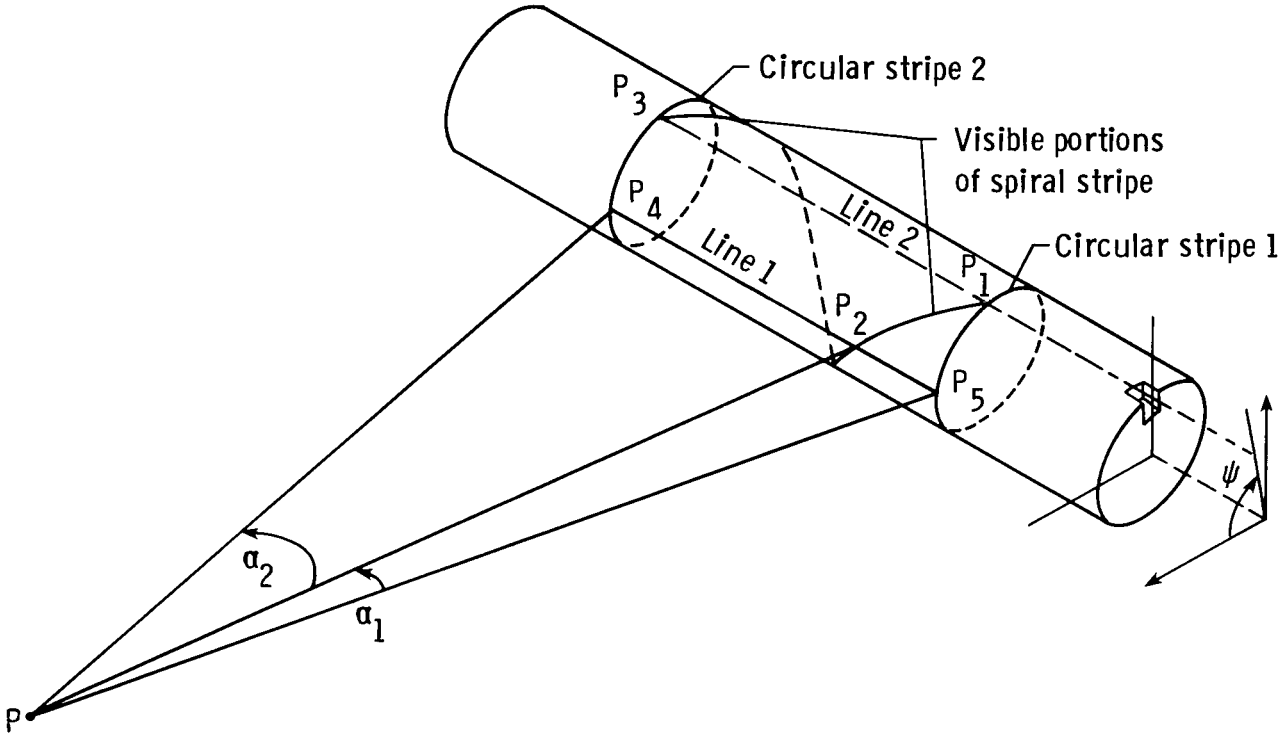

Figure 7.- Rotation of cylinder.

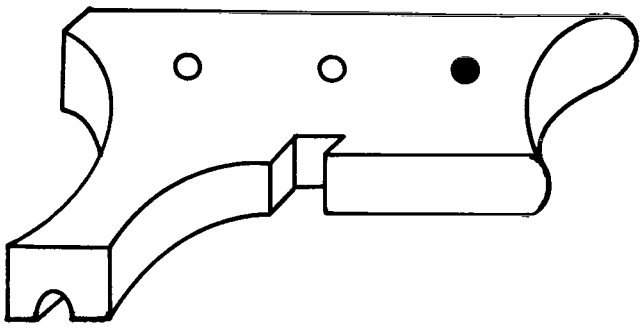

(a) Three-disc marking on a widget.

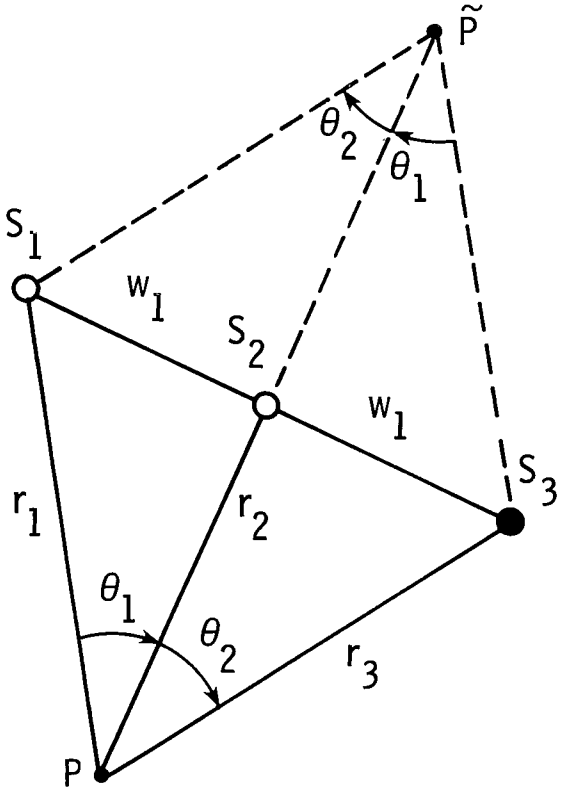

(b) Geometry of three-disc marking.

Figure 8.- Illustration and geometry of three-disc marking.

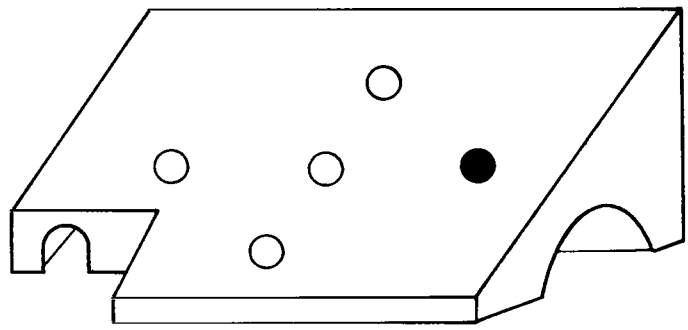

(a) RO + 1 mark on widget.

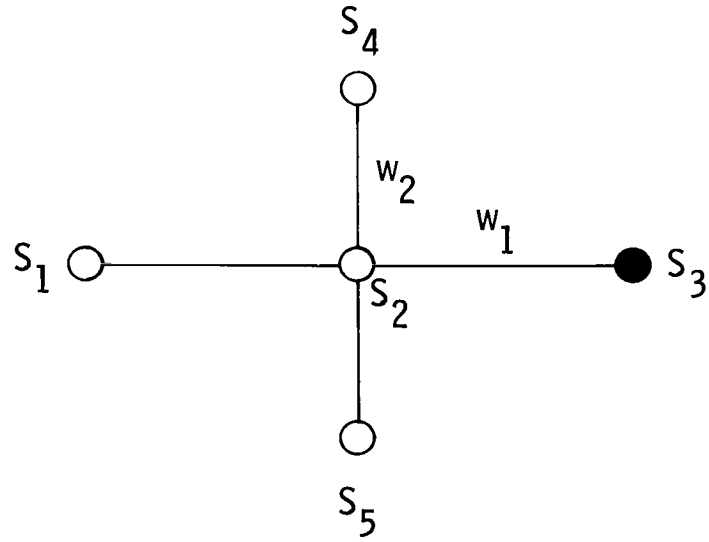

(b) Geometry of RO + 1 mark.

Figure 9.- Illustration and geometry of RO + 1 mark.

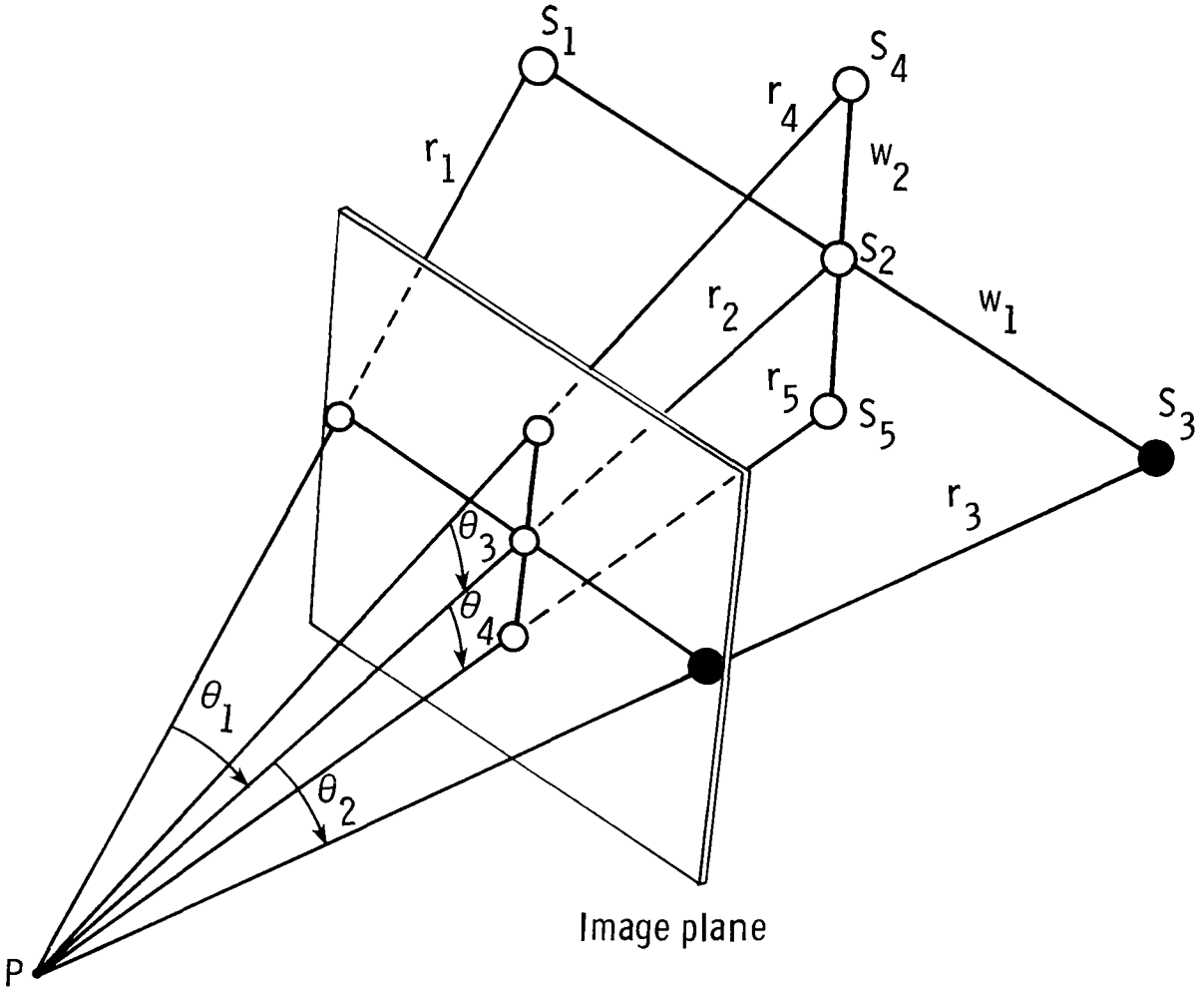

(c) Projection on image plane of RO + 1 mark.

Figure 9.- Concluded.

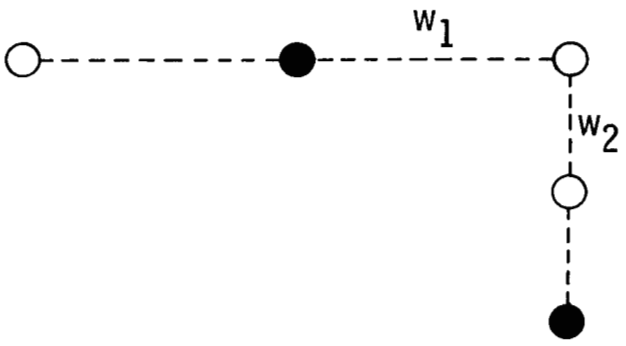

Figure 10.- RO + 2 mark for flat surfaces.

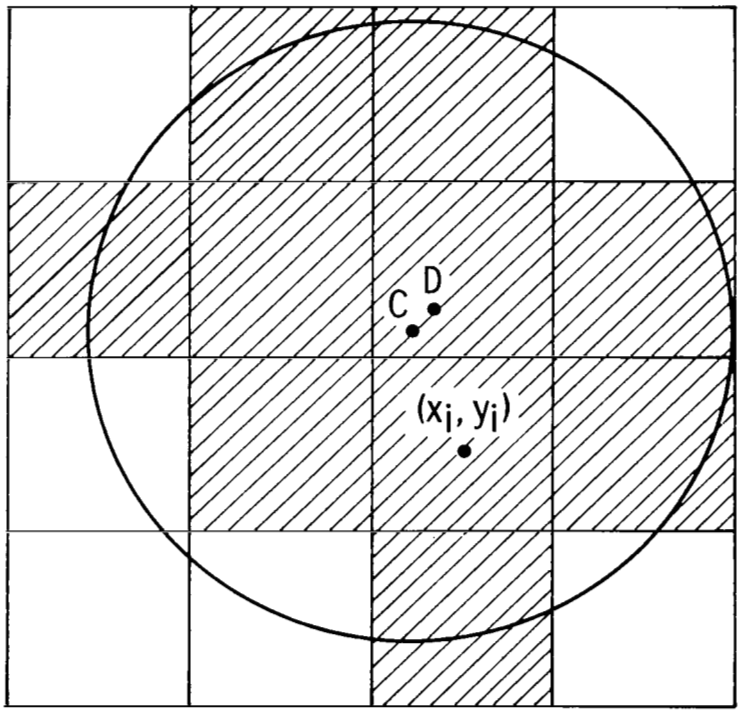

C : Center of circle
D : Centroid of illuminated pixels

Figure 11.- Pixel image of circular disc.

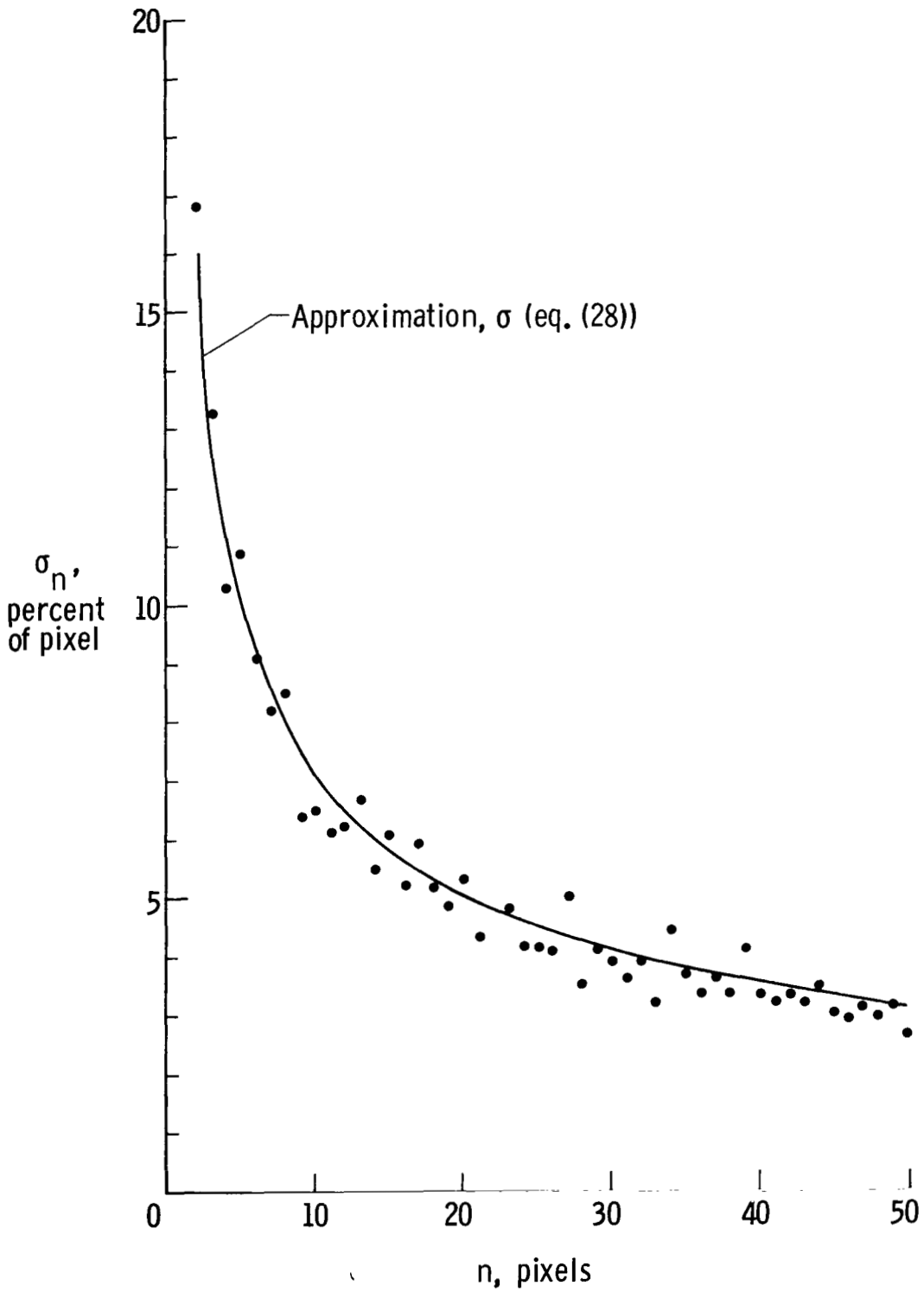

Figure 12.- Standard deviation of $\bar{x}$ component of centroid from x_c.

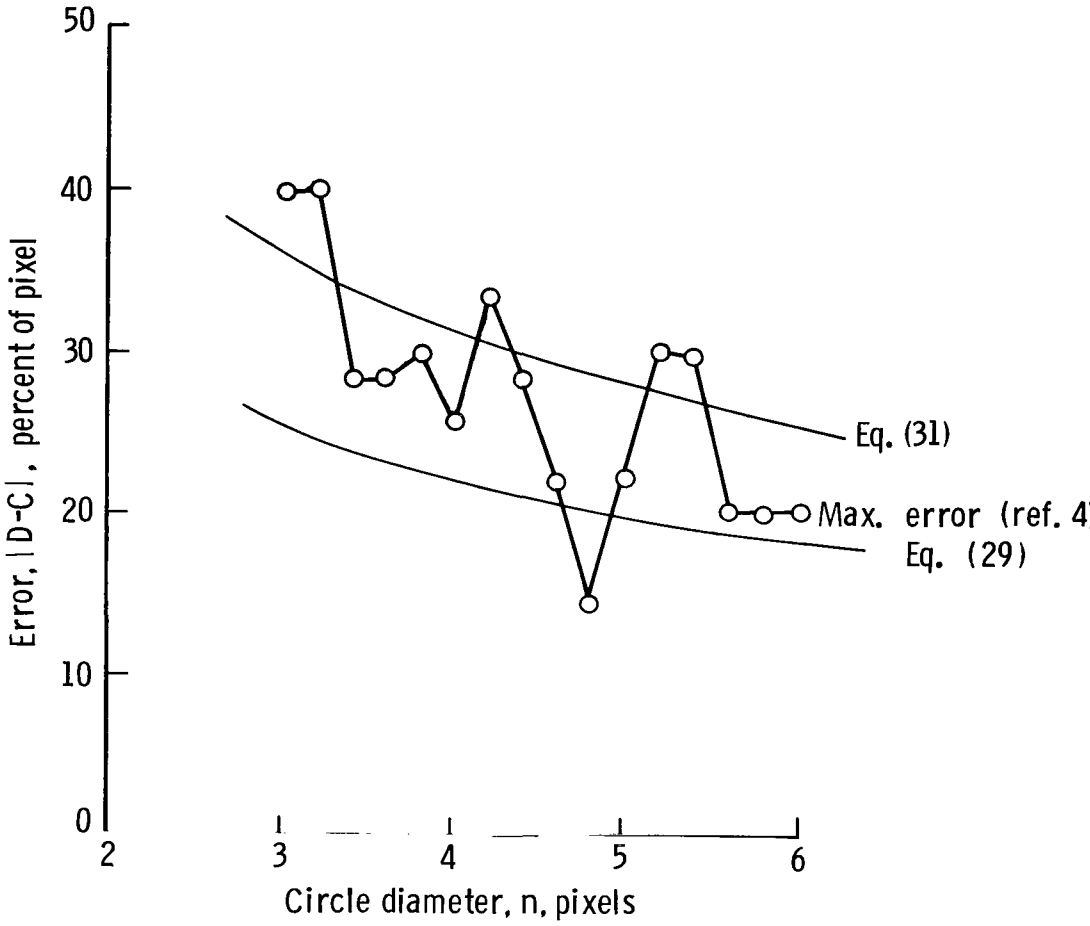

Figure 13.- Location error of circular image center versus size.

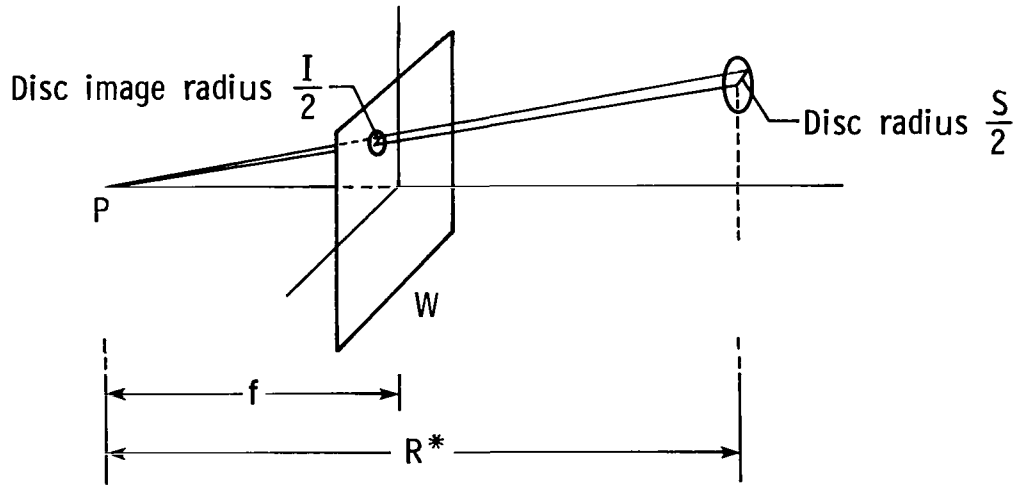

Figure 14.- Illustration of disc and its image.

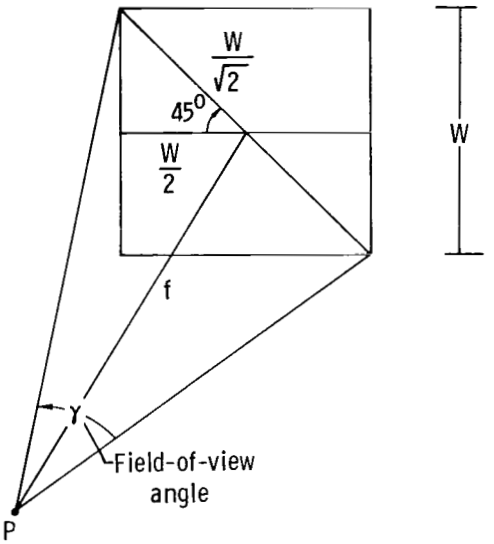

Figure 15.- Illustration of angular field of view measured on diagonal of image plane.

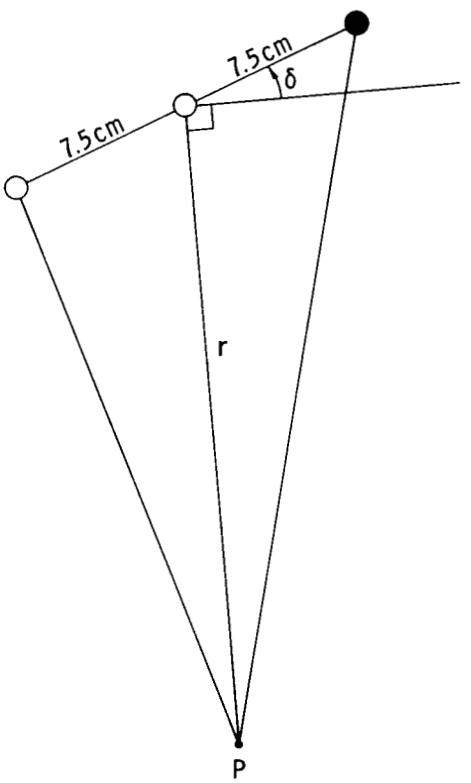

Figure 16.- Range and tilt of three-disc marking.

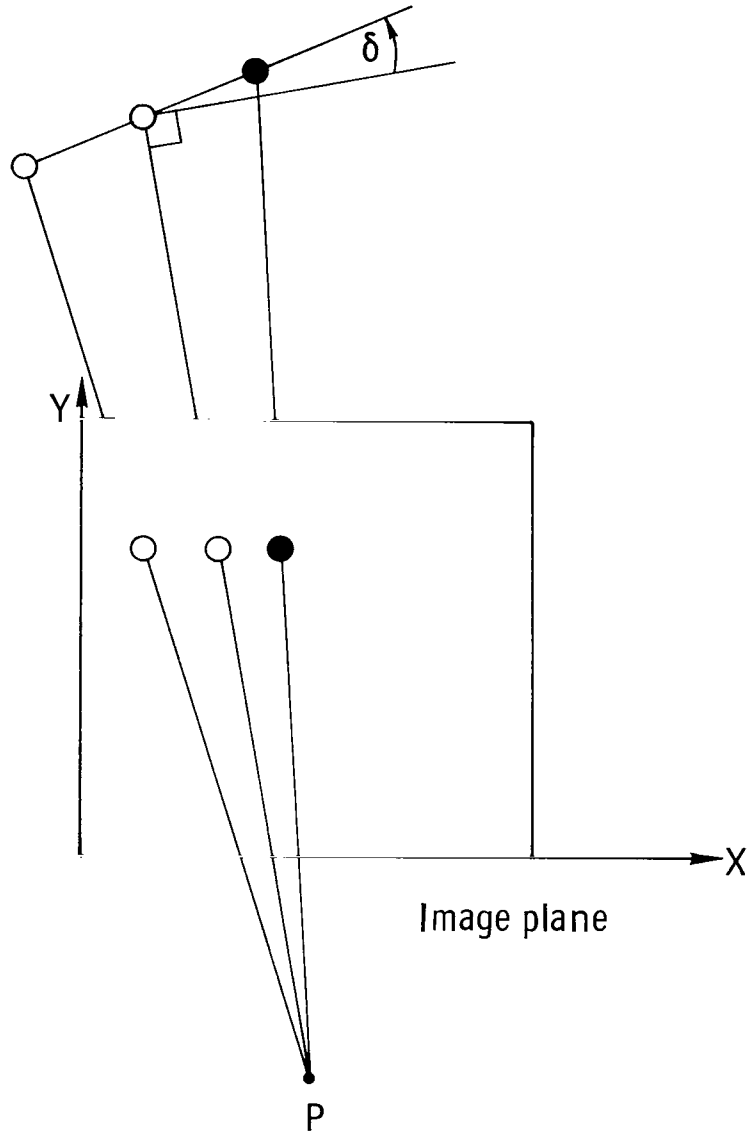

Figure 17.- Image of three-disc marking in the image plane.

1. Report No.	2. Government Accession No.	3. Recipient's Catalog No.
NASA TP-1819		

4. Title and Subtitle	5. Report Date
MARKING PARTS TO AID ROBOT VISION	April 1981
	6. Performing Organization Code 506-54-13-02

7. Author(s)	8. Performing Organization Report No.
John W. Bales and L. Keith Barker	L-14055
	10. Work Unit No.

9. Performing Organization Name and Address	11. Contract or Grant No.
NASA Langley Research Center Hampton, VA 23665	
	13. Type of Report and Period Covered Technical Paper
12. Sponsoring Agency Name and Address National Aeronautics and Space Administration Washington, DC 20546	14. Sponsoring Agency Code

15. Supplementary Notes

John W. Bales: Tuskegee Institute, Participant in the 1980 NASA-Hampton Institute Summer Research Fellowship Program.

L. Keith Barker: Langley Research Center.

16. Abstract

The premarking of parts for subsequent identification by a robot vision system appears to be beneficial as an aid in the automation of certain tasks, such as construction in space. Accordingly, a simple, color-coded marking system is presented which allows a computer vision system to locate an object, calculate its orientation, and determine its identity. Furthermore, such a system has the potential to operate accurately, and, because the computer shape analysis problem has been greatly simplified, it has the potential to operate in real time.

17. Key Words (Suggested by Author(s))	18. Distribution Statement
Automation Robot vision Computer vision Color-coded parts Marking parts	Unclassified - Unlimited Subject Category 59

19. Security Classif. (of this report)	20. Security Classif. (of this page)	21. No. of Pages	22. Price
Unclassified	Unclassified	33	A03

For sale by the National Technical Information Service, Springfield, Virginia 22161

NASA-Langley, 1981

3 1 1U,G, 032781 S00903DS
DEPT OF THE AIR FORCE
AF WEAPONS LABORATORY
ATTN: TECHNICAL LIBRARY (SUL)
KIRTLAND AFB NM 87117